Fusion Engineering and Design 161 (2020) 111898

Contents lists available at ScienceDirect

Fusion Engineering and Design

journal homepage: www.elsevier.com/locate/fusengdes

AC loss and contact resistance of different CICC cable patterns: Experiments and numerical modeling

Anvar V.A.[a,b,*], J. Qin[c], Y. Wu[c], T. Bagni[a], A. Devred[d], T.J. Haugan[e], M.S.A. Hossain[b,f], C. Zhou[a,c,*], A. Nijhuis[a,*]

[a] University of Twente, Faculty of Science & Technology, 7522 NB, Enschede, The Netherlands
[b] Institute for Superconducting and Electronic Materials, University of Wollongong, Wollongong, Australia
[c] Institute of Plasma Physics, Chinese Academy of Sciences, Hefei, China
[d] CERN, Technology Department, CH-1211, Geneva 23, Switzerland
[e] US Air Force Research Laboratory, Wright Patterson AFB, OH, 45433, USA
[f] School of Mechanical and Mining Engineering, the University of Queensland, Brisbane, QLD, 4072, Australia

ARTICLE INFO

Keywords:
JackPot ACDC
Electromagnetic Modeling
Superconducting cables
LTS
Nuclear fusion
CFETR
ITER
DEMO
AC loss
Contact resistance

ABSTRACT

For upcoming nuclear fusion energy reactors, like the China Fusion Engineering Test Reactor (CFETR) and EU-DEMO, the superconducting Cable-In-Conduit Conductors (CICC) are in the design phase, and the operating conditions like electromagnetic forces can be higher than in previous devices like ITER. The prototype conductors for the Central Solenoid (CS) coils in the CFETR, for example, are designed to produce a peak field of 19.9 T and are expected to be made of high current density Nb_3Sn strands. Investigations are also ongoing on the application of bismuth strontium calcium copper oxide (BSCCO) and MgB_2 strands for CICCs in fusion reactors. The latter material, MgB_2, could be applied for superconductors subjected to lower magnetic fields, such as Poloidal Field coils, Correction Coils, and Feeders. The performance of all these strands is sensitive to strain, and the mechanical strength of the brittle filaments is relatively weak. This requires a thorough analysis of the cable pattern in terms of the mechanical support of the strands along their length in combination with the minimization of the interstrand coupling currents and strand indentation. As an initial step to finding the most appropriate cable pattern for CICCs, three prototype CICCs made of ITER type Nb_3Sn strands with significantly different cable twist patterns are tested experimentally for AC coupling loss, interstrand contact resistance, and strand indentation. The three cabling patterns referred to as the Twente, CWS (copper wound superconducting strand), and CFETR-CSMC (CFETR Central Solenoid Model Coil) design. The numerical code JackPot ACDC developed at the University of Twente is used to analyze the interstrand coupling loss and contact resistance. The new ASIPP (Institute of Plasma Physics, Chinese Academy of Sciences) triplet modified CWS design is aimed at reducing strand pinching during cabling, which causes degradation of transport properties during compaction and cyclic loading. The Twente design has the same objective but also aims at reducing the coupling loss while maximizing the mechanical lateral support for the strands by making the twist pitch ratio of the sequential cabling stages close to one. The CFETR-CSMC, taken as a reference for comparison, has cable a pattern mostly similar to the ITER CS cable design.

1. Introduction

Superconducting cables play a vital role in achieving stable high magnetic fields required in nuclear fusion power plants. The CFETR, which stands for “China Fusion Engineering Test Reactor,” is a new tokamak device to be built in China as a complementary to ITER (International Thermonuclear Experimental Reactor), presently being built in Europe. Also, in Europe, the design activities are ongoing for ITER's successor, DEMO, a DEMOnstration fusion power plant [1]. Their magnet systems include Toroidal Field (TF), Central Solenoid (CS), Poloidal Field (PF), Correction Coils (CC), and Feeders. The operating conditions for the superconducting Cable-In-Conduit-Conductors (CICCs) can be more severe than ever before. For example, the CS coil system of the CFETR consists of eight modules with a combination of low-temperature Nb_3Sn strands and high-temperature Bi-2212 to generate a maximum magnetic field of 19.9 T at 51.25 kA/turn [2].

* Corresponding authors at: University of Twente, Faculty of Science & Technology, 7522 NB Enschede, The Netherlands.
E-mail addresses: v.a.anvar@utwente.nl (V.A. Anvar), chao.zhou@ipp.ac.cn (C. Zhou), a.nijhuis@utwente.nl (A. Nijhuis).

https://doi.org/10.1016/j.fusengdes.2020.111898
Received 5 April 2020; Received in revised form 25 June 2020; Accepted 18 July 2020

While the PF, CC, and Feeder materials operate at lower magnetic fields. For future fusion reactors, bismuth strontium calcium copper oxide (BSCCO) [3] and rare-earth barium copper oxide (REBCO) [4,5] materials are being considered for the high magnetic field coils. For conductors operating in a lower magnetic field, MgB_2 could be a potential candidate because it provides a more significant temperature margin or higher operating temperature [6]. The superconducting cables for all magnet coil systems are considered to adopt the CICC concept.

CICCs consist of a certain number of superconducting and copper strands transposed and twisted together in a rope-like pattern and inserted into a steel jacket. A typical void fraction (VF) of around 30 % is maintained for forced flow helium circulation to have adequate cooling. A central hole or helium flow pressure relief channel is mostly also provided.

Since the advent of the CICC concept [7], many studies have been performed to optimize the cabling design for low AC loss, mechanical strength against electro-mechanical forces, low cabling degradation, higher current sharing temperature (T_{cs}), higher engineering current density, high-voltage insulation, efficient cooling, and pressure loss reduction of supercritical helium flow [8–11]. Present-day research mainly focuses on two features besides cost reduction: transverse load stability and reducing AC losses. Although also, other superconducting materials such as the REBCO and BSCCO with potential for high-field (TF and CS) and MgB_2 for low-field (PF) are of interest. The design variables that influence the cable stiffness, strand support, and AC loss apart from the strand surface properties, stiffness, and diameter are cable void fraction, twist pitch pattern, and shape of the cable cross-section (aspect ratio).

Most of the research work on CICC cable concepts have occurred in the field of magnets for nuclear fusion reactors [12–17]. As a result, ITER has set a standard baseline for all magnet types: the Central Solenoid Model Coil (CSMC) [18], Poloidal Field Coil Insert (PFCI) [19], and Toroidal Field Model Coil (TFMC) [20]. For high field magnets above 6 T, Nb_3Sn is the commercially used strand material. Nb_3Sn is brittle and sensitive to strain, so eventual cracks in the filaments lead to irreversible degradation of the transport properties [21–24]. High strain sensitivity and brittleness can lead to poor conductor performance due to fatigue loads in electro-magnetic cycling [25–27]. In 2010, it was observed that the CS conductor performance degraded at only around 10 % of the required reactor plasma operating current pulses [28–30]. This poor performance would have a drastic influence on the practical lifetime of a fusion plant. In 2006, the computation model TEMLOP helped to better understand, predict, and prevent transverse load degradation of CICCs [31]. The most important conclusion was that an adequate increase or decrease of the cabling twist pitch length, thereby reducing local stress concentrations in strands crossovers, could solve the problem of severe degradation. This prediction was later confirmed by experiments in the SULTAN facility [32]. In the case of CS conductors, the research and development program for the development of Toroidal Field coils for ITER (R&D ITER TF) development strategy of longer twist pitches was not put to use because of suspected higher AC losses from alternating magnetic fields and currents [25]. According to the classical supposition, the coupling loss increases roughly with the square of the twist pitch length if the contact resistance (R_c) remains constant. Such a simplified principle is not suitable to analyze the behavior of complicated CICC cable patterns. The JackPot ACDC model, specially developed at the University of Twente to study ITER CICCs [33–37], predicted that a conductor with relatively long twist pitch patterns starting from above 100 mm and in particular keeping the twist pitch ratio of the subsequent stages slightly above one, will still have relatively low coupling losses [38]. An experimental test later confirmed this result in the SULTAN facility [37,39].

The usual strand coating for Nb_3Sn to avoid sintering of strands and to reduce the coupling currents is chromium. A highly resistive chromium strand coating reduces the current sharing between strands. The reduction of current sharing reduces the coupling loss component of the total AC loss in the cable. If an ultra-high resistive strand coating like in [40] is not favored to minimize the coupling loss in so-called Short Twist Pitch (STP) cables such as the present solution for the ITER CS-type [8,41], a twist pitch scheme with a twisting stage ratio close to one could be suitable if AC loss is a critical design parameter. A significant advantage of a longer twist pitch in the first cabling stage in combination with a twist pitch sequence ratio close to one (TPR1) is the minimal deformation (bending and pinching) of the strands. The void fraction should be reduced to minimize the strand movement in TPR1 cable patterns, which will slightly affect the thermo-hydraulics of helium circulation [42]. Reducing the void fraction for a specific cable twist pitch pattern increases the transverse cable stiffness [31]. However, it also results in a higher coupling loss time constant, which eventually is reduced somewhat with cyclic loading, although the scope of reduction depends on the void fraction [41,43]. For a CICC with sufficient cable stiffness and lateral strand support, the scope for strand movement in the bundle is restricted. Therefore, the increase of interstrand contact resistance during cyclic loading is expected to be also limited.

In order to understand the effects of cabling variations, three cabling patterns with different twist pitches have been studied for AC loss and interstrand contact resistance. The CICC samples were manufactured from Nb_3Sn strand. However, the comparisons in terms of coupling loss and strand mechanical deformation are considered relevant for other materials such as BiSCCO and MgB_2 round wires as well. For evaluation and comparison of the three different conductor designs, the interstrand coupling losses and contact resistances were analyzed with the numerical code JackPot ACDC, and also the strand deformation was examined post-mortem. The correlation between the numerical code and experimental results for the different cabling configurations should demonstrate the ability of the code to predict the performance of unconventional cabling patterns.

2. Experiments and modeling

2.1. AC loss measurements

The AC loss of the prototype cables was measured with a sinusoidal magnetic field applied perpendicular to the long axis of the conductor in the AC dipole facility at the University of Twente [34–36]. AC loss and interstrand contact resistance experiments are done on heat-treated samples. Fig. 1 shows the different components and connections of the AC dipole facility. The AC loss is measured by two methods: gas flow calorimetry and pick up (PU) coil magnetization [44,45].

Gas flow calorimetry measures the power dissipation in the conductor utilizing a calibrated gas flow of boil-off helium. A heater inside the sample chamber is used for calibrating the calorimetric measurements. The calorimeter is inserted in the bore of a superconducting dipole magnet. The measurements are done with and without an offset magnetic field and carried out at 4.2 K in a liquid helium bath at atmospheric pressure. The pick-up coil magnetization method uses two pick-up coils, one around the sample (PU) and one empty correction coil (CC). Both signals are subtracted and integrated over time to construct the magnetization loops representing the total loss per cycle.

2.2. CFETR Prototypes – cabling patterns

Three different cabling patterns were examined. The first one is the copper-wound superconducting strand (CWS) design, which is proposed to reduce the strand indentation in STP cabling as observed in the tightly compacted ITER CS type conductors. The STP design possesses higher stiffness and better performance for cyclic loading, although the small crossover angles result in deep strand indentations. In the CWS type, a soft copper strand is wound around the two superconducting

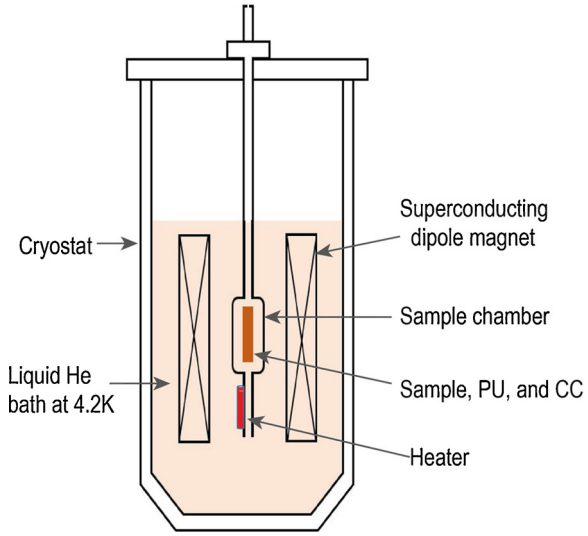

Fig. 1. Schematic diagram of the AC dipole facility.

strands (SC) in the first stage to reduce the indentation in the SC strands. The twist pitch of the Cu strands in the first stage is four (CWS-I) to five (CWS-II) times smaller than that of the SC strands in the same triplet. The CWS concept essentially should maintain the stiffness of the ITER CS type cable but with reduced strand indentations [46].

The second cable type is a shorter twist pitch version of the Twente cable design with the subsequent twist pitch ratio close to one. The earlier proposed and tested Twente design concept for the ITER CS type follows a twist pitch ratio slightly above one with a first stage twist pitch of 110 mm (110 × 118 × 126 × 140 × 352) [37]. The first stage twist pitch of the Twente design tested here is about half that of the previous design to preserve sufficient stiffness. However, there are some changes in the manufactured cable and original proposed CWS and Twente design. The void fraction of the Twente design is accidentally reduced from the original intended 27 to 23 % after manufacturing. For both cables, Twente and CWS, the petal wrap coverage is reduced from the original target of 70 to 45 %. Both these changes have a significant impact on the cable performance, specifically for the coupling loss. The impact of these changes is described in this paper. Post-mortem analysis of the cable is also done to check the strand indentation from cabling and compaction.

The third cable design used for the CFETR CSMC conductor is serving as a baseline for comparison. The CFETR CSMC has the same cable pattern as the ITER CS STP conductor except for the final stage. The so-called initial slope coupling loss time constant is found from the initial and steep slope of the experimentally determined AC loss versus frequency curve for a sinusoidal applied magnetic field. For ITER CS conductors, this is generally in the range of 300 − 700 ms [46].

2.2.1. Sample details, preparation, and measurement

The three CICC conductors tested here have a round-in-square geometrical configuration in which Nb_3Sn strands are cabled (with right-hand twist direction) as six petals with a multistage round cable pattern inside a square steel jacket (316 L N). All three cables were made from ITER type strands of the same diameter produced by Western Superconducting Technologies Co., Ltd., Xi'an, China (WST). One-third of them, 288 strands, among a total of 864 strands, were made of copper [46]. The basic cable pattern and overall conductor parameters are given in Table 1. The cabling angle (cos Θ) is determined for all cable types with the help of the JackPot ACDC model [35], considering SC strands only. The cos Θ can be used in case the absolute volume needs to be calculated.

Each conductor sample was mounted with a pick-up coil (PU, coil area perpendicular to the magnetic field) and a compensation coil (CC, parallel to and in-plane with the pick-up coil and near the sample) to measure the sample magnetization simultaneously with the calorimetric data [47]. Calorimetric flow measurements require a certain time to settle depending upon the helium gas flow rate, the circuit flow resistance and involved volumes even though voltage signals respond quickly to any gas flow changes. Disregarding previous AC cycles needed to reach a stable gas flow rate, for each magnetic field frequency and amplitude setting, the final five calorimetric and magnetization loops were recorded for accuracy, and the average value is taken. Fig. 2 shows the various parts of the prepared CICC with mounted PU and CC coils inserted in a calorimeter.

The measured AC loss was normalized per total volume of Nb_3Sn strands. The length of the samples used was 40 cm, and the diameter of each strand element was 0.82 +/-0.005 mm. A volume of 576 Nb_3Sn strands was taken, giving 121.7 cm^3, for the AC loss normalization of the conductor. The average SC strand angle from Table 1 was not considered for calculation of the exact volume. The magnitude of the AC loss is calculated from the measured area of the magnetization loop. The magnetization measurement is calibrated with the calorimetric measurement. Sinusoidal modulation field of 150 m T with and without a background field of 350 m T is used for the AC loss measurement.

2.3. Interstrand contact resistance (R_c) measurement

The contact resistance is an essential factor in determining the coupling loss in the cable. Predicting the R_c value is difficult due to its dependency on the twist pitch pattern, cable compaction, strand material composition, and coating process, and primarily because the strand surface properties determining the R_c are not known in advance. Here, R_c is defined as the overall resistance value between two selected strands along the measured sample length. The contact frequency within the cable is not uniform, which makes short sample testing not archetypal. However, here, the length of the cable (400 mm) tested is almost comparable to the final stage twist pitch (450 mm) of the cable, and the shorter twist pitches already went through many repetitions. Hence, the measured resistance is considered representative for longer length cables of the same type. Since the resistance measured is for parallel contact, the values are normalized by multiplying them with the length of the cable sample (not length of strands) and reported with unit '$n\Omega.m$.'

The R_c measurements between selected strands were carried out after the AC loss measurements. In this study, the contact resistance measurements are carried out on reacted samples. The jackets of all three cables were cut 5 cm from one of the ends to access the strands for R_c measurements. Great care was taken in preparing the samples since the Nb_3Sn filament material is brittle and sensitive to damage by small movements. None of the selected strands were removed from its twisted configuration for sample preparation, that is to say, the strands remained intact and in their original position.

All the tested cables had five stages of cabling with six petals in the last stage, although the selected strands were tagged as within a petal (intra-petal) or between petals (inter-petal). A total of 14 strands were chosen from the outer petal perimeter, such that two to three random strands are from each petal, as shown in Fig. 3.

One of the prepared samples and the schematic diagram of the current and voltage tap connections are shown in Fig. 4. The chromium coating on the strand surface was removed with abrasive paper before soldering the voltage taps and current leads. Ends of NbTi wires were soldered to the ends of the selected Nb_3Sn strands in the cable. The other NbTi wire ends were soldered to a thick copper current-carrying wire for each strand combination. The reason for using NbTi wires for current transfer was to ease the process of soldering and to avoid local heating of the Nb_3Sn strands. Thin copper wires were used for voltage taps, which were placed at a distance varying from 5 to 20 mm from the current lead contact, which is longer than the current transfer length [48]. The suitable positions for voltage taps were also checked

Table 1
Details of the three Nb_3Sn CICC prototypes, each with a length of 400 mm.

	CWS-I	Twente	CFETR CSMC
Cable pattern	(2Sc + 1Cu) x 3 × 4 × 4 × 6		
Twist pitch length [mm]	(40 + 10) x60 × 90 × 160 × 450	50 × 58 × 66 × 76 × 450	25 × 50 × 90 × 160 × 450
Void fraction [%]	33.2	23	32.9
Cable outer diameter [mm]	32.7	30.5	32.7
Strand diameter [mm]	0.82 ± 0.005 mm		
Cos θ (average strand angle)	0.95	0.93	0.93
Petal wrap coverage [%]	45	45	70
Conduit dimensions [mm]	52 × 52	52 × 52	49 × 49

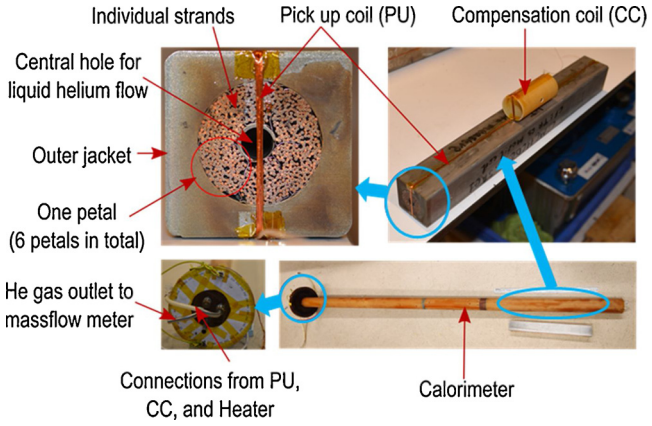

Fig. 2. Details of the prepared CICC conductor sample for AC loss measurement.

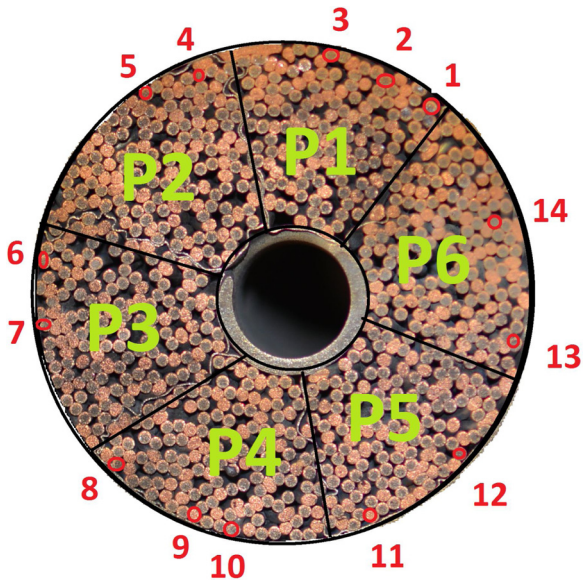

Fig. 3. Petal and strand selection for contact resistance measurement.

experimentally by placing them relatively near and far from the current leads to determine the minimum distance for avoiding current entrance effects. The measurements were carried out under similar conditions as for the AC loss measurements: in a liquid helium bath at 4.2 K and ambient pressure.

The slope of the *V-I* curve is used to determine the contact resistance. As a check for linearity, the current was increased and decreased in steps of 5 A from zero to a maximum of 30 A.

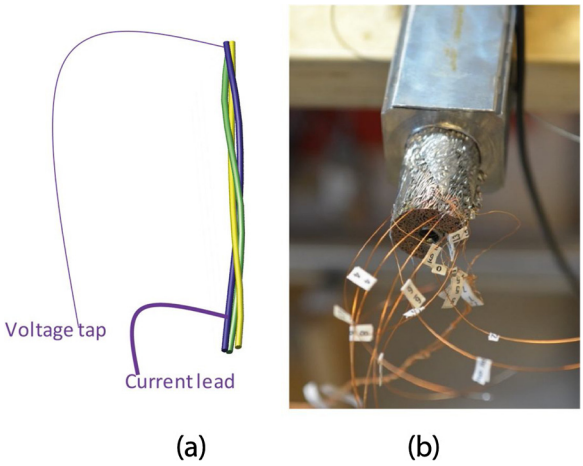

Fig. 4. (a) Schematic diagram and (b) prepared CWS-I conductor sample showing current and voltage tap connections for contact resistance measurement.

2.4. JackPot – numerical network model

For the evaluation of the cable design, the numerical model JackPot ACDC was used. JackPot-ACDC considers the trajectories of all superconducting and copper strands of the cable for building the electrical network model [35,49]. The main feature of JackPot is the cable geometrical model, which is capable of including thousands of strands. The one-dimensional (1D) strands elements altogether make a three-dimensional (3D) geometry reproducing the actual CICC cable pattern. The interstrand contact resistance (R_c) network is calculated using the interstrand contact areas obtained from the geometry and the interstrand resistivity. The resistivity is calibrated using the experimental contact resistance measurements. The network model then finds the voltage at each node along the strand length by calculating self and mutual inductances based on the transport current, self and background field (B), and temperature (T). Strand properties are assigned in the model based on the strand critical current $I_c(B, T, \varepsilon)$ scaling law, with ε representing the axial strain, and the power-law voltage-current relationship of superconducting to normal transition. There are no fitting parameters in the model. The only unknown parameter is the thermal axial strain [50] in the Nb_3Sn filaments due to cool-down, which is taken as -0.5 % [30]. Coupling losses in all the CFETR prototype cables were calculated using realistic R_c distributions based on an extensive experimental database available at the University of Twente. Previous research works show that JackPot can predict the CICC behavior accurately if the contact resistance and strain are known (like in all previous Jackpot works).

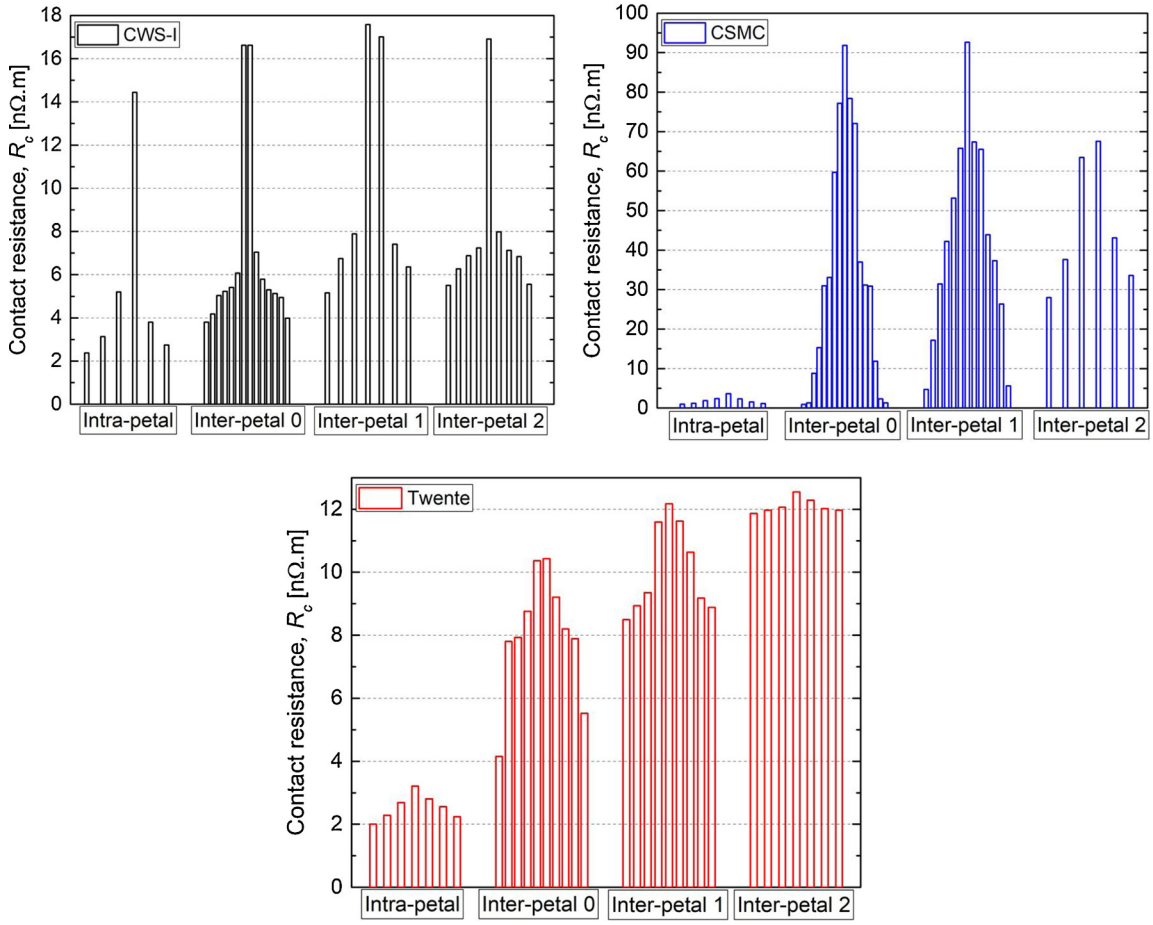

Fig. 5. Interstrand contact resistance measurement results of three cable prototypes.

3. Results and discussion

3.1. Interstrand contact resistance measurement

The intra-petal R_c represents the resistance between the SC strands within a petal. Fig. 5 shows the measured intra-petal and inter-petal contact resistances (R_c) for all three cable prototypes, and they are all within the expected range based on previous test results [51]. The inter-petal R_c refers to the resistance between SC strands from two different petals with that specific number of petals in between, i.e., '*inter-petal 0*' stands for R_c between neighboring petals and '*inter-petal 2*' stands for R_c between petals that have two petals in between them. The additional resistance in the inter-petal R_c is mainly due to the stainless-steel wrap coverage around each of the six petals. The petal wrap coverage for an ITER CS conductor is 70 %, and in fact, all three conductors were supposed to have similar petal wrap coverage of 70 % for a fair comparison. Here, both CWS-I and Twente cables have petal wrap coverage of only 45 %, while the CFETR CSMC has 70 %. The implication of this variation in the cable parameter is visible in Fig. 5.

The results in Fig. 5 show two features in particular: a large spread in inter-petal R_c and a very-low inter-petal R_c for the CWS-I and Twente cables. The spread within a petal is from selecting random strands from the first four stages. The spread in inter-petal R_c, however, is likely from strong uneven contact between petals, as shown in Fig. 6. The red circles in Fig. 6 show direct contact between petals 1 and 2, and the green circle shows the presence of petal wrap between petals 2 and 3, preventing direct contact between the strands in the petals. This non-uniformity in contacts was observed in all three of the measured cables. The petal wrap was removed from the exposed portion of the cable to connect current and voltage taps, as shown in Fig. 6.

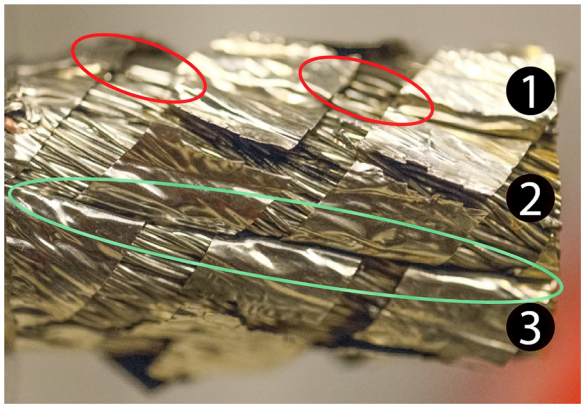

Fig. 6. Non-uniform contact between petals from the petal wrap coverage of the CSMC CICC prototype conductor.

The average inter-petal resistance measured between Cu strands in the CWS-I conductors was 12.2 nΩm, which is relatively low. Chromium coating on the surface of the strands is to avoid strand sintering during the heat treatment process, and this coating increases R_c between strands. Damage to the chromium coating, the deep strand indentations due to the small twist pitch and severe compaction explains the low R_c between Cu strands.

The low inter-petal R_c for the CWS-I and Twente cable prototypes is due to the unintended petal wrap coverage of 45 instead of 70 % and the lower void fractions. In order to make a fair comparison for the different cable patterns, a method will be introduced further on to compensate for these unintended differences.

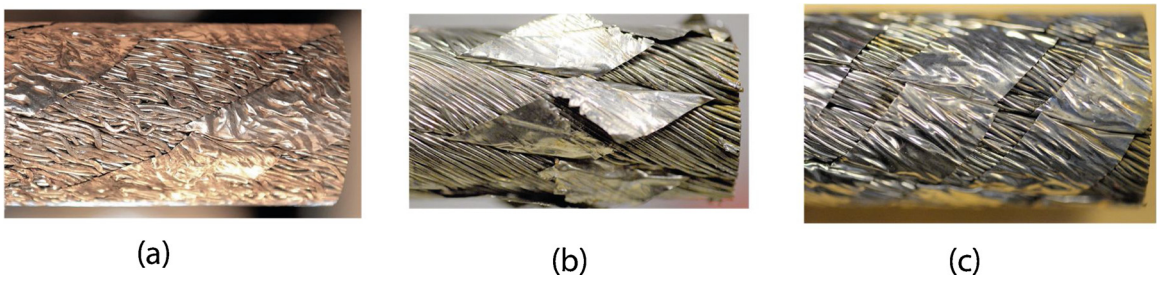

Fig. 7. (a) CWS-I (b), Twente, and (c) CFETR CSMC samples with a section of the steel jacket cut for R_c measurements, showing stainless steel wraps around petals and the differences in strand trajectories.

The reduced petal wrap coverage implies more direct contact between strands of neighboring petals and thus lowers R_c. A reduced R_c will lead to and increased current sharing between strands, and the resulting low resistive current loops in the last cabling stage will increase the coupling loss significantly. In Fig. 7, the typical differences between the cable options can be seen, with the strands much more aligned in the Twente design and least in the CWS-I design, where strands are most severely deformed.

Interstrand R_c simulations were conducted with the JackPot model, and one example of the results is shown in Fig. 8. In order to replicate the R_c experiment, random strands were chosen within a petal and between petals for calculating intra-petal and inter-petal R_c, respectively, following the method of the experimental measurement. As shown in Fig. 8(b), the strand currents start decaying from the connected current lead at the end of the cable by sharing current with all neighboring strands. The current carried by both selected strands at the other end is zero as expected. The current carried by each of the 862 surrounding strands (flat lines in Fig. 8(b)) is comparatively low due to the large number of them. The red (+) and blue dot (-) in Fig. 8 (a) shows the location of the selected strands, and the length of the simulated cable section is the same for all, 0.4 m, just as in the experiment.

Average values of all experimental data were taken compared to the JackPot R_c simulations of the three cable prototypes in Fig. 9. The R_c distribution based on the experiments is then used for the JackPot coupling loss simulation. The R_c values of the experimental measurement and JackPot simulation are also listed in Table 2.

3.2. AC loss

Fig. 10 shows the loss-frequency dependence of the Twente prototype cable obtained by calorimetry and magnetization in perpendicular applied magnetic AC field. The calorimetric and magnetization data are in fair agreement. For the given field amplitude and frequency range, the AC loss for Nb_3Sn CICCs is generally higher without background field (offset) as compared to the loss measured with background field due to both smaller penetration field and magnetoresistance of copper, although the difference is rather small.

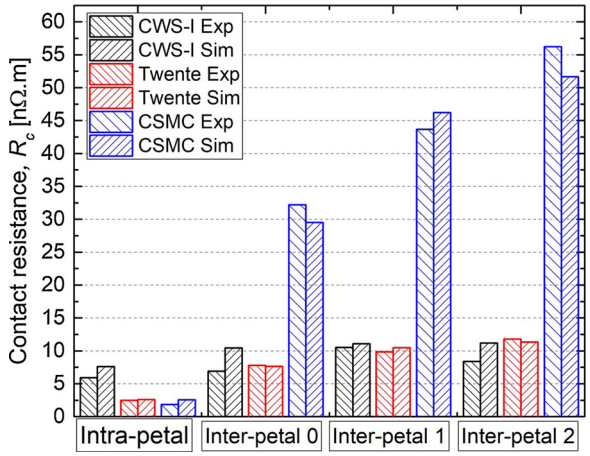

Fig. 9. Comparison of results from experimental measurements and JackPot simulations of the average R_c in the three cable prototypes.

A third-order polynomial function fits the loss-frequency dependencies obtained by magnetization for the CWS conductor and a second-order for both the Twente and the CFETR CSMC cables. Irrespective of the degree of the fitting polynomial (not shown in Fig. 10), the y-intercept values are used for the calculation of hysteresis losses, and the linear coefficient of the fitted curve is used for the calculation of the coupling loss time constant, $n\tau$. The fitting is not used to modify the experimental data nor to make a comparison with JackPot analysis.

The coupling loss time constant $n\tau$ is obtained from the initial slope of the loss-frequency curve [47]:

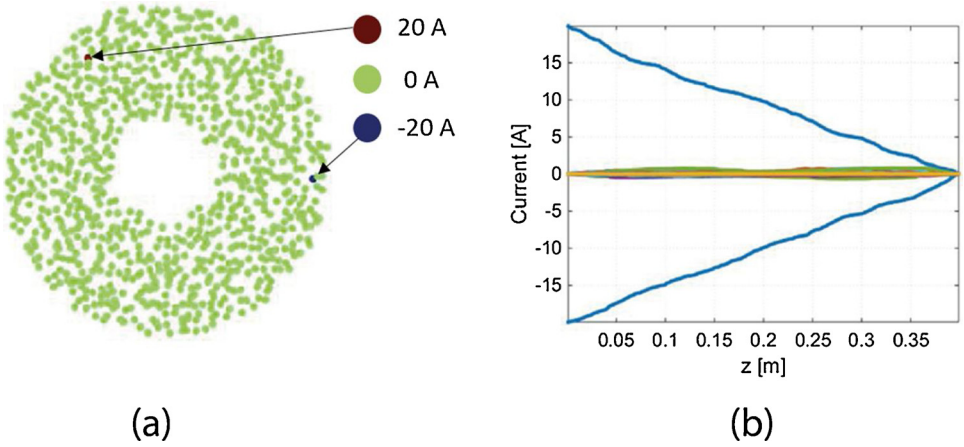

Fig. 8. JackPot modeling of an R_c measurement, showing (a) selection of strands and (b) current sharing between all 864 strands along the cable length (z).

Table 2
Average interstrand contact resistance values from the experimental measurements and JackPot simulations of the three cable prototypes.

	CWS-I		Twente		CFETR CSMC	
	Experiment [nΩ.m]	JackPot Sim	Experiment	JackPot Sim	Experiment	JackPot Sim
Intra-petal	5.9	7.6	2.5	2.6	1.8	2.7
Inter-petal 0	6.9	10.5	7.8	7.7	32.2	29.5
Inter-petal 1	10.5	11.1	9.8	10.5	43.7	46.2
Inter-petal 2	8.4	11.2	11.8	11.3	56.2	51.6

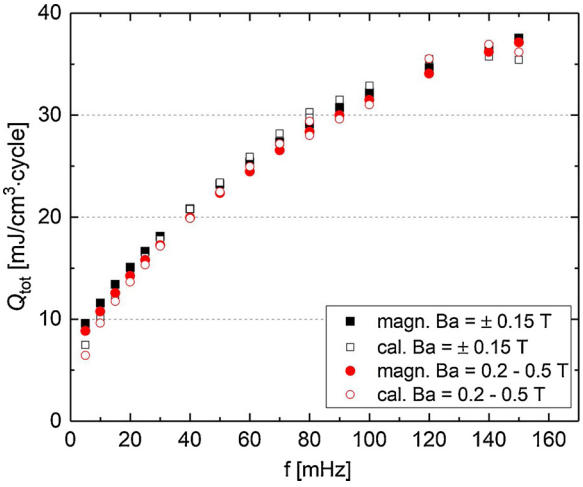

Fig. 10. The total AC loss-frequency dependence from magnetization and calorimetric measurements on the Twente cable design (all experimental data are without any curve fitting, B_a is the magnitude of the applied AC magnetic field).

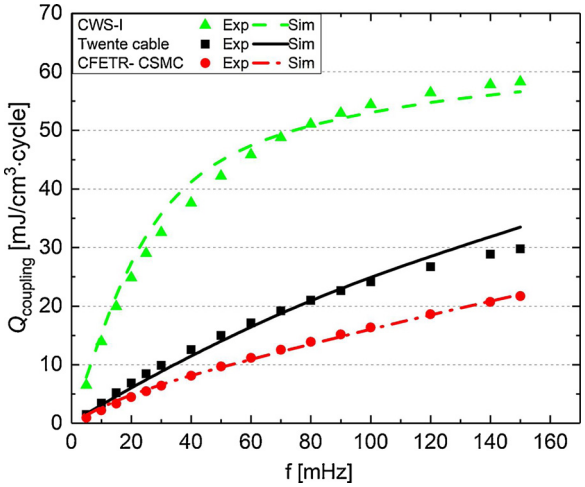

Fig. 11. Comparison of coupling loss for experimental measurements and JackPot simulations based on the R_c values determined above, for the three cable prototypes.

$$n\tau = \alpha \frac{\mu_0}{2\pi^2 {B_a}^2} \quad (1)$$

Where B_a is the amplitude of the magnetic AC field. The loss curve slope, which is described as a constant 'α ' of the right-hand side of (1), is determined from the initial slope at low frequencies. However, the single time constant fails to describe the coupling loss over an extended range of frequencies [47,52,53] since many time constants are present in multi-stage cables. For this reason, a simulation with JackPot is more accurate for specific magnetic fields and current variations. The value of the coupling loss time constant, $n\tau$ is used here to compare the AC loss of the different cables. Since the $n\tau$ value is calculated for the same frequency range for all the cables, it gives a proper basis for comparison of the AC loss behavior of different cables irrespective of the nτ dependence on the frequency range. The total loss is a combination of coupling loss and hysteresis loss. The coupling loss is dependent and the hysteresis loss is independent on the frequency of the applied AC field. So, in theory, approaching zero frequency only hysteresis loss is present in the cable. Hence the hysteresis loss is calculated from the AC loss-axis intercept of the loss versus frequency curve.

Coupling loss simulations with JackPot were conducted at 4.2 K without transport current. For comparison with the experimental data, only the case without the background field is simulated. The results of both the AC loss experiments and the simulations are shown in Fig. 11. The intra-strand coupling losses are negligible in the experimental frequency range [37].

The hysteresis loss (Q_{hys}), the initial slope of the AC loss curve (α), and the coupling loss time constant ($n\tau$) of all three samples are listed in Table 3. Here B_a is the applied AC magnetic field, and B_{dc} is the DC background magnetic field.

The hysteresis loss of both the Twente and the CFETR CSMC cables is in the same range, while the CWS-I shows a slightly higher value. This difference might be due to the inaccuracy related to the steep initial slope of the loss versus frequency curve for the CWS-I sample. The presence of the background field B_{dc} reduces the Q_{hys} as expected. As compared to the CFETR CSMC, the $n\tau$ value of the Twente cable is 1.6 times higher, and that of the CWS-I is 5.5 times higher.

Table 3
Experimental loss-frequency parameters of all three cable prototypes with $B_{ap}{}_1 = B_{dc} + B_a$.

B_a [T]	B_{dc} [T]	CWS-I	Twente	CFETR CSMC
		Q_{hys} [mJ cm^{-3}]		
± 0.15	0	10.5 ± 0.8	7.7 ± 0.1	7.5 ± 0.1
	0.35	9.1 ± 0.6	6.9 ± 0.1	7.2 ± 0.1
		α [J.s/m^3 × 10^6]		
± 0.15	0	1.48 ± 0.07	0.409 ± 0.006	0.274 ± 0.006
	0.35	1.36 ± 0.07	0.402 ± 0.005	0.244 ± 0.005
		$n\tau$ [ms]		
± 0.15	0	4190 ± 200	1157 ± 17	775 ± 17
	0.35	3850 ± 140	1137 ± 14	690 ± 14

Transverse resistivity between petals depends on petal wrap coverage, petal diameter, relative arrangement of wraps in neighboring petals, and cable compaction. When the inter-petal to intra-petal R_c ratio is high, the coupling loss contribution is mainly generated inside the petals. A recent study [46] showed a strong dependence between the coupling loss time constant, $n\tau$ and the intra-petal R_c. However, the inter-petal to intra-petal R_c ratio of the Twente conductor tested here is ~11 due to low petal wrap coverage, and for the CWS-I conductor tested here is ~1 due to the combination of low petal wrap coverage and high cable compaction. This low R_c ratio leads to a significant increase in inter-petal coupling losses in both cables as shown in Fig. 12. A four-fold reduction in the coupling loss is reported for a CICC conductor with wraps compared to that without wraps (VF = 34 %, 1440

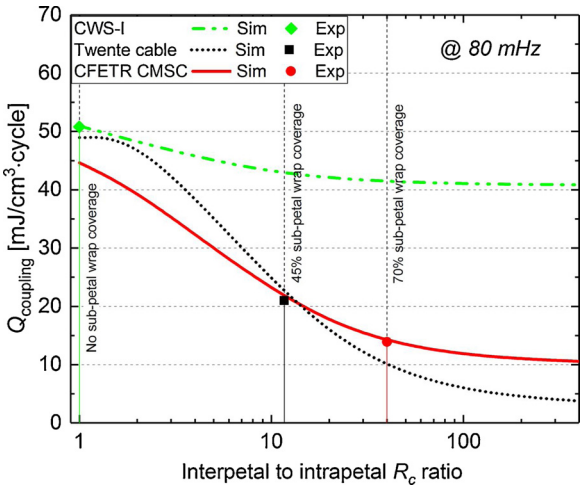

Fig. 12. Jackpot simulation showing the effect of the inter-petal to intra-petal R_c ratio on coupling losses in the CFETR CSMC cable (the lines are simulation data and the thick points are experimental data).

NbTi strands) [54]. Here the computed coupling loss at no petal wrap coverage is three times higher than 70 % petal wrap coverage for CFETR CSMC. The simulation was done with a sinewave applied magnetic field at frequency of 80 mHz, and applied field amplitude of 150 m T), where the value of $n\tau$ is significant. The percentage of petal wrap coverage is simulated by changing the inter-petal to intra-petal R_c ratio. The ratio becomes one when there is no petal wrap coverage.

The coupling loss increase for lower R_c ratios is drastic, but it saturates at higher ratios for the simulated frequency of 80 mHz and chosen cable configuration. Fig. 12 also shows that the coupling loss reduces with increasing inter-petal to intra-petal R_c ratio, confirming that the petal wrap coverage of 70 % is more effective than 45 % in reducing the total coupling loss in all the three cable types, although the impact for CWS-I is marginal. The values of petal wrap coverage corresponding to the inter-petal to intra-petal R_c ratio shown in Fig. 12 are from experiments and simulations done on the cables studied in this work. Here two main cable parameters are playing significant roles in the observed results for Twente and CWS-I cable in comparison with CFETR CSMC; petal wrap coverage and void fraction.

3.2.1. Effect of petal wrap coverage

The local inter-petal R_c will be practically the same as the intra-petal R_c where adjacent petals are in direct contact without any wrap in between. Typical petal wrap coverages for ITER conductors are in the range of 70 % for CS, and 50 % for TF and PF CICCs [19,55]. Petal wrap coverage of both Twente and CWS-I cables was 45 %, and of CFETR CSMC was 70 %. Simulations show that the Twente cable has practically similar coupling loss as the CFETR CSMC cable at a petal wrap coverage of ~ 45 % but significantly less coupling loss at 70 %. However, at lower inter-petal to interstrand coverage, the Twente cables show higher coupling loss than the CFETR CSMC because the coupling loss component from the last cable stage becomes dominant. Last stage (stage 5) twist pitch length of all cables is 450 mm (Table 1), so at inter-petal to intra-petal R_c approaching 1 (no petal wraps), coupling losses of all cables approach to almost similar values. The remaining difference is due to variation in the twist pitch scheme of the first four cable stages.

A broader petal wrap coverage also reduces local buckling of strands on the petal surface [56]. However, increasing the petal wrap coverage or transverse resistivity between petals beyond a specific limit can have negative consequences on the cable performance, such as lower cooling rates and reduced current sharing. However, as for the main argument of current sharing between petals and reduction of DC performance, research has shown that cables with and without petal wraps show similar current distribution behavior at least until ten times the I_c criterion of 10 μV/m. The local peak voltages caused by non-uniform current distribution within the petals of NbTi CICCs can lead to an earlier quench [57]. A petal wrap coverage of 70 % allows for the required current sharing and helium exchange between the petals [30]. The JackPot simulations also show that increasing beyond 70 % petal wrap coverage is less effective in reducing the coupling loss in the cable for all three cables tested.

3.2.2. Effect of the void fraction (VF)

Cable compaction or reducing the VF decreases both inter-petal and intra-petal R_c [58]. The concept of a threshold VF was first discussed in a paper published in 2001, though not explicitly stated. Upon compacting a cable beyond a certain VF, the coupling loss drastically increases due to the loss contribution from the last stage of the cable. The last stage has longer twist pitch length and hence higher coupling loss, this is usually reduced by a highly resistive stainless-steel wrap around the last stage i.e., petal. The last stage coupling loss becomes dominant only if the petal wraps are ineffective. The VF at which the petal wraps become ineffective in limiting the last stage coupling loss is referred to as threshold VF. Although the change in inter-petal R_c is not significant up to a certain VF in the case of high resistive wrap coverage, compacting the cable beyond a threshold VF value can have similar effects to that of no petal wraps [59]. It was found for an Nb_3Sn CICC with 60 % petal wrap coverage that the coupling loss time constant increases dramatically below 24 % VF due to the effect of compaction [59]. The last stage coupling loss becomes dominant below a certain VF, a behavior that was observed in conductors without petal wraps due to increased current sharing between the petals [59,60]. The VF at which the compaction threshold for inter-petal coupling loss is reached, likely also depends on the percentage of petal wrap coverage, twist pitch length, and cabling pattern. Compacting a cable increases the cable stiffness, but with compaction, the strands are pressed against each other, and indentations at strand crossovers damage the strands [58], which is detrimental to the cable performance. So, there is an optimum window of VF for each cable design.

Even though the petal wrap coverage of the CWS-I cable is 45 %, the combined experimental and computed results (Fig. 12) indicate performance similar to that of no petal wraps. Due to peculiarity in the first stage of the CWS-I cable design, the sliding of strands is limited hence making the cable stiffer even at higher VF. Strands are less flexible to move during compaction and are almost locked; the resulting petal deformation and transverse pressure reduce the inter-petal R_c significantly. This makes the petal wraps ineffective in reducing coupling loss in the same way as in [58], exceeding the VF threshold. A manufacturing difficulty of CWS-I cable is also experienced at the cable compaction stage at ASIPP, China. Post-mortem examination of the CWS-I cable showed highly deformed petal wraps and strands. All these lead to the conclusion that CWS-I cable already reached its VF threshold value for inter-petal R_c at or above a VF of 33.2 %.

The Twente cable follows a design strategy of cable stage twist pitch ratio close to 1 (TPR1). For the TPR1 type of cables, the strands are mostly parallel to each other forming line contacts, which is efficient for the optimized filling of voids inside the jacket and creating lateral strand support. So even at a VF of 23 %, the cable did not reach the threshold VF value for inter-petal coupling loss, but the reduction in VF certainly affects coupling loss. The coupling loss analysis of ITER TF and CS model coil conductors for different VF's at 4.2 K, with 150 m T amplitude and 350 m T background stationary field shows that the coupling loss increases almost linearly with the reduction of the VF in the range of interest [58]. This indicates that for these types of prototype ITER conductors, strand movement was still possible, and depending on the cabling twist pitch scheme, mechanically stable CICCs should have low void fraction but not exceeding the inter-petal coupling loss VF threshold. It is not obvious to calculate the inter-petal R_c values from petal wrap coverage percentage alone due to its

Table 4
Contact resistance values used in the JackPot simulations.

	CWS-I [10^{-12} Ω. m^2]	Twente	CFETR CSMC
Intra-petal R_c	0.8	0.3	0.35
Inter-petal R_c	0.9	3.5	15
Inter-petal R_c calculated	32	12	~

dependence on VF and relative arrangement of wrap coverage between petals.

The reduction in petal wrap coverage (70 to 45 % in Twente cable and CWS-I) and VF (27 % to 23 % in Twente cable) together contributed to the observed high coupling loss. In order to assess the reduction of the inter to intra-petal R_c ratio, another simulation is done but now with a similar R_c ratio as in the case of the CFETR CSMC cable. The modified inter-petal resistance of CWS-I and Twente conductors is calculated by multiplying the inter-petal to intra-petal R_c ratio of CFETR CSMC (~40) with intra-petal R_c of CWS-I and Twente conductors. The obtained inter-petal R_c values used in the JackPot simulation are shown in Table 4.

Fig. 13 shows the JackPot simulation results with the predicted AC losses as a function of frequency for an inter-petal to intra-petal R_c ratio for both the Twente and the CWS-I conductors representing ~70 % petal coverage, taken as that of the CFETR CSMC cable. The JackPot simulation indicates that the coupling loss of the Twente design will be reduced considerably and become less than the CFETR CSMC cable loss. Though the coupling loss of CWS-I design has reduced, it is still significantly higher than the other two cables.

In contrast to both CWS-I and CFETR CSMC conductor designs, no visible strand indentations are found on the extracted strands from the Twente design sample despite the exceptionally small void fraction, as shown in Fig. 14. The Twente cable pattern is therefore very suitable for strain sensitive wire materials. Severe indentation on Cu and SC strands in CWS-I cable also damaged the resistive chromium coating, which further reduced the contact resistance.

It is confirmed that the cable pattern, petal wraps, and void fraction significantly affect the coupling loss. The primary purpose of this work is to address the influence of the cable pattern on the coupling loss and strand indentation. It is demonstrated that the Twente cable pattern with twist pitch ratio close to one, has the lowest coupling loss and the least strand deformation, even with a first stage triplet twist pitch which is twice that of the CSMC and also larger than that of the CWS-I.

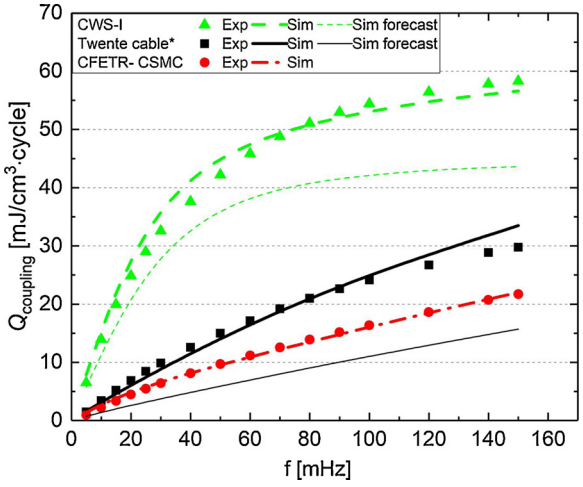

Fig. 13. Predicted coupling losses of the Twente and CWS-I cables for similar wrap coverage as compared to the CSMC cable (70 instead of 45 %). (The lines in the figure refer to the simulations while the symbols are for the experimental data).

4. Conclusion

The AC loss and interstrand contact resistance have been measured on three prototype Nb_3Sn Cable-In-Conduit Conductors with significantly different cabling twist pitch patterns. In the CWS cable, a soft copper strand is wound around the two superconducting strands (SC) in the first stage with twist pitch five times smaller than that of the SC strands in the same triplet to reduce the indentation of the SC strands. The second cable type is a shorter twist pitch version of the Twente cable design concept with the subsequent twist pitch ratio close to one. The CFETR CSMC has the same cable pattern as the ITER CS STP conductor except for the final stage. Simulations, done by using the JackPot model are in fair agreement, confirming the consistency of data and allowing reliable predictions with the JackPot model. Simulations have been performed to compare the performance of the different cable designs; this confirms that a design petal wrap coverage of 70 % should be maintained for CS cables to reduce the AC loss.

The experiments and simulations of AC loss and contact resistance conducted in this study confirm previous research from others that a critical threshold value of void fraction exists, which makes the presence of petal wraps ineffective in reducing coupling loss (from the CWS-I cable results). For the copper wound superconducting strand short twist pitches design, this threshold is already reached at or above 33 %, while for the Twente design, the limit was still not reached at 23 % void fraction.

The JackPot simulations with derived corrections for inter-petal contact resistance representing 70 % petal wrap coverage show that the Twente cable design has the lowest coupling loss. Internal post-mortem examination of the conductors revealed no visible strand indentation for the Twente design, even at a void fraction of 23 %, opposite to both other designs, with a most severe indentation for the CWS-I type even damaging the Cr plating. So far, the Twente cable design seems a suitable candidate for CFETR or DEMO conductors, made of strain-sensitive strands such as Nb_3Sn or other materials, for minimization of coupling loss and strand indentation. However, studies are continued for further optimization.

CRediT authorship contribution statement

Anvar V.A.: Data curation, Formal analysis, Investigation, Software, Validation, Visualization, Writing - original draft. **J. Qin:** Conceptualization, Formal analysis, Funding acquisition, Resources. **Y. Wu:** Conceptualization, Formal analysis, Funding acquisition, Resources. **T. Bagni:** Data curation, Software, Validation, Visualization, Writing - review & editing. **A. Devred:** Formal analysis, Funding acquisition. **T.J. Haugan:** Conceptualization, Formal analysis, Funding acquisition, Resouces. **M.S.A. Hossain:** Formal analysis, Funding acquisition, Supervision. **C. Zhou:** Conceptualization, Formal analysis, Funding acquisition, Resources, Writing - review & editing. **A. Nijhuis:** Conceptualization, Formal analysis, Funding acquisition, Methodology, Project administration, Supervision, Validation, Writing - review & editing.

Declaration of Competing Interest

The authors declare that they have no known competing financial interests or personal relationships that could have appeared to influence the work reported in this paper.

Acknowledgments

This work was supported by the National Key R&D program of China (Grant No. 2017YFE0301404), and in part, supported by the National Natural Sciences Foundation of China (Grant No. 51677184). The U.S. Department of Energy under contract numbers DE-SC0014009

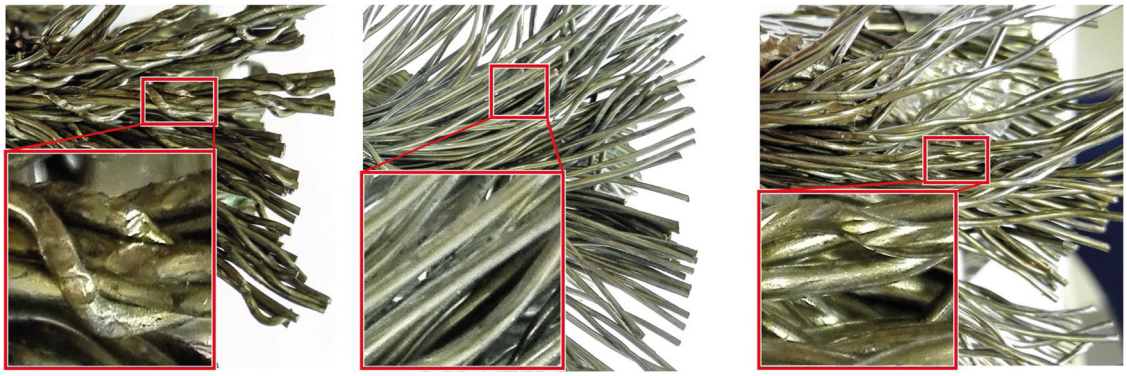

Fig. 14. Examination of strands from (a) CWS-I, (b) Twente, and (c) CFETR CSMC samples after AC loss and R_c experiments to investigate strand indentations, with higher magnification shown in the insets.

and DE-SC0015775 support part of the work. We also received support from the Air Force Office of Scientific Research (AFOSR)LRIR #14RQO8COR, and the Aerospace Systems Directorate (AFRL/RQ), the Air Force Office of Scientific Research (AFOSR) through LRIR # 18RQCOR100, and the Aerospace Systems Directorate (AFRL/RQ). This work was also partially supported by the Australian Research Council Linkage Project (LP160101784). The views and opinions expressed herein do not necessarily reflect those of any of the above-acknowledged parties.

Appendix A. Supplementary data

Supplementary material related to this article can be found, in the online version, at doi:https://doi.org/10.1016/j.fusengdes.2020.111898.

References

[1] D. Uglietti, K. Sedlak, R. Wesche, P. Bruzzone, L. Muzzi, A. della Corte, Progressing in cable-in-conduit for fusion magnets: from ITER to low cost, high performance DEMO, Supercond. Sci. Technol. 31 (2018) 055004.
[2] Y. Wan, J. Li, Y. Liu, X. Wang, V. Chan, C. Chen, X. Duan, P. Fu, X. Gao, K. Feng, S. Liu, Y. Song, P. Weng, B. Wan, F. Wan, H. Wang, S. Wu, M. Ye, Q. Yang, G. Zheng, G. Zhuang, Q. Li, Overview of the present progress and activities on the CFETR, Nucl. Fusion 57 (2017).
[3] J. Qin, Y. Shi, Y. Wu, J. Li, Q. Wang, Y. He, C. Dai, F. Liu, H. Liu, Z. Mao, A. Nijhuis, C. Zhou, A. Devred, First AC loss test and analysis of a Bi2212 cable-in-conduit conductor for fusion application, Supercond. Sci. Technol. 31 (2018) 015010.
[4] D. Uglietti, A review of commercial high temperature superconducting materials for large magnets: from wires and tapes to cables and conductors, Supercond. Sci. Technol. 32 (2019) 053001.
[5] D.C. van der Laan, J.D. Weiss, D.M. McRae, Status of CORC ® cables and wires for use in high-field magnets and power systems a decade after their introduction, Supercond. Sci. Technol. 32 (2019) 033001.
[6] G. Giunchi, B. Coppi, MgB2 coil options for fusion poloidal magnets, IEEE Trans. Appl. Supercond. 20 (2010) 1610–1613.
[7] M. Hoenig, D. Montgomery, Dense supercritical-helium cooled superconductors for large high field stabilized magnets, IEEE Trans. Magn. 11 (1975) 569–572.
[8] L. Muzzi, G. De Marzi, A. Di Zenobio, A. Della Corte, Cable-in-conduit conductors: lessons from the recent past for future developments with low and high temperature superconductors, Supercond. Sci. Technol. 28 (2015) 053001.
[9] P. Bruzzone, 30 years of conductors for fusion: a summary and perspectives, IEEE Trans. Appl. Supercond. 16 (2006) 839–844.
[10] J.L. Duchateau, D. Ciazynski, O. Guerber, S.H. Park, W.H. Fietz, A. Ulbricht, G. Zahn, L. Zani, Exploring the limits of a very large Nb 3 Sn conductor: the 80 kA conductor of the international thermonuclear experimental reactor toroidal field model coil, Supercond. Sci. Technol. 17 (2004) S241.
[11] L. Dresner, Superconductor stability, 1983: a review, Cryogenics (Guildf). 24 (1984) 283–292.
[12] J. Wei, W.G. Chen, W.Y. Wu, Y.N. Pan, D.M. Gao, S.T. Wu, Y. Wu, The superconducting magnets for EAST tokamak, IEEE Trans. Appl. Supercond. 20 (2010) 556–559.
[13] B.S. Lim, S.I. Lee, J.Y. Choi, W. Chung, Y. Chu, H.K. Park, K.M. Kim, S.Y. Kim, B.S. Kim, Development of CICC for KSTAR TF coil system, IEEE Trans. Appl. Supercond. 13 (2003) 1496–1499.
[14] S. Ishida, P. Barabaschi, Y. Kamada, Status and prospect of the JT-60SA project, Fusion Eng. Des. 85 (2010) 2070–2079.
[15] N. Mitchell, A. Devred, P. Libeyre, B. Lim, F. Savary, The ITER magnets: design and construction status, IEEE Trans. Appl. Supercond. 22 (2012) 4200809.
[16] T. Rummel, K. Rieße, H. Ehmler, Manufacture and test of the non-planar coils for WENDELSTEIN 7-X, Fusion Eng. Des. 75–79 (2005) 117–121.
[17] F. Hosono, G. Iwaki, S. Inaba, T. Suzuki, K. Hiroshima, K. Kikuchi, K. Chida, M. Watahiki, K. Kamata, S. Pradhan, Y.C. Sazena, Production of NbTi CICC's for SST-1 project at IPR, IEEE Trans. Appl. Supercond. 11 (2001) 2014–2017.
[18] N. Martovetsky, P. Michael, J. Minervini, A. Radovinsky, M. Takayasu, C.Y. Gung, R. Thome, T. Ando, T. Isono, K. Hamada, T. Kato, K. Kawano, N. Koizumi, K. Matsui, H. Nakajima, G. Nishijima, Y. Nunoya, M. Sugimoto, Y. Takahashi, H. Tsuji, D. Bessette, K. Okuno, N. Mitchell, M. Ricci, R. Zanino, L. Savoldi, K. Arai, A. Ninomiya, Test of the ITER central solenoid model coil and CS insert, IEEE Trans. Appl. Supercond. 12 (2002) 600–605.
[19] D. Bessette, L. Bottura, A. Devred, N. Mitchell, K. Okuno, Y. Nunoya, C. Sborchia, Y. Takahashi, A. Verweij, A. Vostner, R. Zanino, E. Zapretilina, Test results from the PF conductor insert coil and implications for the ITER PF system, IEEE Trans. Appl. Supercond. 19 (2009) 1525–1531.
[20] A. Ulbricht, J.L. Duchateau, W.H. Fietz, D. Ciazynski, H. Fillunger, S. Fink, R. Heller, R. Maix, S. Nicollet, S. Raff, M. Ricci, E. Salpietro, G. Zahn, R. Zanino, M. Bagnasco, D. Besette, E. Bobrov, T. Bonicelli, P. Bruzzone, M.S. Darweschsad, P. Decool, N. Dolgetta, A. della Corte, A. Formisano, A. Grünhagen, P. Hertout, W. Herz, M. Huguet, F. Hurd, Y. Ilyin, P. Komarek, P. Libeyre, V. Marchese, C. Marinucci, A. Martinez, R. Martone, N. Martovetsky, P. Michael, N. Mitchell, A. Nijhuis, G. Nöther, Y. Nunoya, M. Polak, A. Portone, L. Savoldi Richard, M. Spadoni, M. Süßer, S. Turtú, A. Vostner, Y. Takahashi, F. Wüchner, L. Zani, The ITER toroidal field model coil project, Fusion Eng. Des. 73 (2005) 189–327.
[21] A. Godeke, A review of the properties of Nb3Sn and their variation with A15 composition, morphology and strain state, Supercond. Sci. Technol. 19 (2006).
[22] M.C. Jewell, P.J. Lee, D.C. Larbalestier, The influence of Nb 3 Sn strand geometry on filament breakage under bend strain as revealed by metallography, Supercond. Sci. Technol. 16 (2003) 1005.
[23] Y. Miyoshi, E.P.A. van Lanen, M.M.J. Dhalle, A. Nijhuis, Microscopic fractures and transport degradation in ITER type Nb3Sn strands, IEEE Trans. Appl. Supercond. 20 (2010) 1404–1407.
[24] C. Sanabria, P.J. Lee, W. Starch, I. Pong, A. Vostner, M.C. Jewell, A. Devred, D.C. Larbalestier, Evidence that filament fracture occurs in an ITER toroidal field conductor after cyclic Lorentz force loading in SULTAN, Supercond. Sci. Technol. 25 (2012).
[25] D. Bessette, N. Mitchell, Review of the results of the ITER toroidal field conductor R &D and qualification, IEEE Trans. Appl. Supercond. 18 (2008) 1109–1113.
[26] P. Bruzzone, B. Stepanov, R. Wesche, Qualification tests for ITER TF conductors in SULTAN, Fusion Eng. Des. 84 (2009) 205–209.
[27] M. Breschi, A. Devred, M. Casali, D. Bessette, M.C. Jewell, N. Mitchell, I. Pong, A. Vostner, P. Bruzzone, B. Stepanov, T. Boutboul, N. Martovetsky, K. Kim, Y. Takahashi, V. Tronza, Y. Wu, Results of the TF conductor performance qualification samples for the ITER project, Supercond. Sci. Technol. 25 (2012) 95004.
[28] A. Devred, D. Bessette, P. Bruzzone, K. Hamada, T. Isono, N. Martovetsky, N. Mitchell, Y. Nunoya, K. Okuno, I. Pong, W. Reiersen, C.M. Rey, B. Stepanov, Y. Takahashi, A. Vostner, Status of conductor qualification for the ITER central solenoid, IEEE Trans. Appl. Supercond. 23 (2013) 6001208.
[29] T. Hemmi, Y. Nunoya, Y. Nabara, M. Yoshikawa, K. Matsui, H. Kajitani, K. Hamada, T. Isono, Y. Takahashi, N. Koizumi, H. Nakajima, B. Stepanov, P. Bruzzone, Test results and investigation of tcs degradation in japanese ITER CS conductor samples, IEEE Trans. Appl. Supercond. 22 (2012) 4803305.
[30] S. Charlie, J.L. Peter, S. William, D. Arnaud, C.L. David, Metallographic autopsies of full-scale ITER prototype cable-in-conduit conductors after full cyclic testing in SULTAN: III. The importance of strand surface roughness in long twist pitch conductors, Supercond. Sci. Technol. 29 (2016) 74002.
[31] A. Nijhuis, Y. Ilyin, Transverse load optimization in Nb3Sn CICC design; influence of cabling, void fraction and strand stiffness, Supercond. Sci. Technol. 19 (2006)

945–962.
[32] A. Nijhuis, A solution for transverse load degradation in ITER Nb3Sn CICCs: verification of cabling effect on Lorentz force response, Supercond. Sci. Technol. 21 (2008) 54011.
[33] E.P.A. Van Lanen, J. Van Nugteren, A. Nijhuis, Full-scale calculation of the coupling losses in ITER size cable-in-conduit conductors, Supercond. Sci. Technol. 25 (2012).
[34] Y. Miyoshi, G. Rolando, A. Vostner, Y. Nabara, A. Nijhuis, First results of AC loss test on ITER TF conductors with transverse load cycling, IEEE Trans. Appl. Supercond. 22 (2012) 4804304.
[35] E.P.A. van Lanen, A. Nijhuis, JackPot: a novel model to study the influence of current non-uniformity and cabling patterns in cable-in-conduit conductors, Cryogenics (Guildf). 50 (2010) 139–148.
[36] E.P.A. Van Lanen, J. Van Nugteren, A. Nijhuis, Validation of a strand-level CICC-joint coupling loss model, Supercond. Sci. Technol. 25 (2012).
[37] G. Rolando, A. Devred, A. Nijhuis, Minimizing coupling loss by selection of twist pitch lengths in multi-stage cable-in-conduit conductors, Supercond. Sci. Technol. 27 (2014) 015006.
[38] A. Nijhuis, G. Rolando, C. Zhou, E.P.A. van Lanen, J. van Nugteren, R.P.P. van Meerdervoort, H.J.G. Krooshoop, W.A.J. Wessel, A. Devred, A. Vostner, I. Pong, Optimization of interstrand coupling loss and transverse load degradation in ITER Nb3Sn CICCs, IEEE Trans. Appl. Supercond. 23 (2013) 4201206.
[39] Y. Nabara, T. Hemmi, H. Kajitani, H. Ozeki, T. Suwa, M. Iguchi, Y. Nunoya, T. Isono, K. Matsui, N. Koizumi, F. Tsutsumi, Y. Uno, M. Oshikiri, K. Shibutani, Y. Takahashi, K. Okuno, Y. Murakami, T. Miyatake, M. Sugimoto, A. Takagi, Y. Nakada, K. Miyashita, K. Sedlak, B. Stepanov, P. Bruzzone, Impact of cable twist pitch on tcs -degradation and AC loss in Nb3Sn conductors for ITER central solenoids, IEEE Trans. Appl. Supercond. 24 (2014) 1–5.
[40] A. Nijhuis, H.H.J. ten Kate, V. Pantsyrny, M. Santini, Interstrand contact resistance and AC loss of a 48-strands Nb/sub 3/Sn CIC conductor with a Cr/Cr-oxide coating, IEEE Trans. Appiled Supercond. 10 (2000) 1090–1093.
[41] Y. Takahashi, Y. Nabara, H. Ozeki, T. Hemmi, Y. Nunoya, T. Isono, K. Matsui, K. Kawano, M. Oshikiri, Y. Uno, F. Tsutsumi, K. Shibutani, T. Kawasaki, K. Okuno, Y. Murakami, M. Tani, G. Sato, Y. Nakata, M. Sugimoto, Cabling technology of Nb3Sn conductor for ITER central solenoid, IEEE Trans. Appl. Supercond. 24 (2014) 1–4.
[42] A. Brighenti, R. Bonifetto, T. Isono, K. Kawano, G. Russo, L. Savoldi, R. Zanino, Overview of the hydraulic characteristics of the ITER Central Solenoid Model Coil conductors after 15 years of test campaigns, IOP Conf. Ser. Mater. Sci. Eng. 278 (2017).
[43] A. Nijhuis, H.H.J. ten Kate, P. Bruzzone, L. Bottura, Parametric study on coupling loss in subsize ITER Nb,Sn cabled specimen, IEEE Trans. Magn. 32 (1996) 2743–2746.
[44] J.A. Eikelboom, Apparatus for calorimetric measurement of a.c. Losses in superconductors, Cryogenics (Guildf). 31 (1991) 363–365.
[45] A.J.M. Roovers, W. Uijttewaal, H.H.J. ten Kate, B. Ten Haken, L.J.M. Van de Klundert, A loss measurement system in a test facility for high-current superconducting cables and wires, IEEE Trans. Magn. 24 (1988) 1174–1177.
[46] J. Qin, Y. Wu, J. Li, F. Liu, C. Dai, Y. Shi, H. Liu, Z. Mao, A. Nijhuis, C. Zhou, K.A. Yagotintsev, R. Lubkemann, V.A. Anvar, A. Devred, New design of cable-in-conduit conductor for application in future fusion reactors, Supercond. Sci. Technol. 30 (2017) 115012.
[47] A. Nijhuis, H.H.J. Kate, J.L. Duchateau, P. Bruzzone, Coupling loss time constants in full-size Nb3Sn CIC model conductors for fusion magnets, in: L.T. Summers (Ed.), Adv. Cryog. Eng. Mater. Springer, US, Boston, MA, 1996, pp. 1281–1288.
[48] C. Zhou, M. Dhallé, H.H.J. Ten Kate, A. Nijhuis, Current transfer length in multi-filamentary superconducting NbTi and Nb3Sn strands; experiments and models, Supercond. Sci. Technol. 27 (2014).
[49] T. Bagni, A. Devred, A. Nijhuis, Strand level modeling of contact resistance and coupling loss for EU-DEMO-TF prototype conductors, Supercond. Sci. Technol. 32 (2019) 105012.
[50] C. Calzolaio, P. Bruzzone, B. Stepanov, Monitoring of the thermal strain distribution in CICCs during the cyclic loading tests in SULTAN, IEEE Trans. Appl. Supercond. 23 (2013) 4200404.
[51] Y. Shi, J. Qin, Y. Wu, F. Liu, H. Liu, H. Jin, Q. Hao, A. Nijhuis, K. Yagotintsev, C. Zhou, Mechanical and electrical properties of a CFETR CSMC conductor under transverse mechanical loadings, IEEE Trans. Appl. Supercond. 28 (2018) 1–5.
[52] B. Turck, L. Zani, A macroscopic model for coupling current losses in cables made of multistages of superconducting strands and its experimental validation, Cryogenics (Guildf). 50 (2010) 443–449.
[53] T. Bagni, J.L. Duchateau, M. Breschi, A. Devred, A. Nijhuis, Analysis of ITER NbTi and Nb 3 Sn CICCs experimental minimum quench energy with JackPot, MCM and THEA models, Supercond. Sci. Technol. 30 (2017) 95003.
[54] A. Nijhuis, Y. Ilyin, H.H.J. Ten Kate, The effect of inter-bundle resistive barriers on coupling loss, current distribution and DC performance in ITER conductors, IEEE Trans. Appl. Supercond. 16 (2006) 868–871.
[55] C. Sanabria, P.J. Lee, W. Starch, A. Devred, D.C. Larbalestier, S. Charlie, J.L. Peter, S. William, D. Arnaud, C.L. David, Metallographic autopsies of full-scale ITER prototype cable-in-conduit conductors after full cyclic testing in SULTAN: III. The importance of strand surface roughness in long twist pitch conductors, Supercond. Sci. Technol. 29 (2016) 74002.
[56] A. Nijhuis, E.P.A. van Lanen, G. Rolando, Optimization of ITER Nb 3 Sn CICCs for coupling loss, transverse electromagnetic load and axial thermal contraction, Supercond. Sci. Technol. 25 (2012) 15007.
[57] Y. Ilyin, A. Nijhuis, H.H.J. ten Kate, Interpretation of conduit voltage measurements on the poloidal field insert sample using the CUDI–CICC numerical code, Cryogenics (Guildf). 46 (2006) 517–529.
[58] A. Nijhuis, Y. Ilyin, W. Abbas, H.H.J. TenKate, M.V. Ricci, A. DellaCorte, Impact of void fraction on mechanical properties and evolution of coupling loss in ITER Nb3Sn conductors under cyclic loading, IEEE Trans. Appiled Supercond. 15 (2005) 1633–1636.
[59] Y. Takahashi, K. Matsui, K. Nishii, N. Koizumi, Y. Nunoya, T. Isono, T. Ando, H. Tsuji, S. Murase, S. Shimamoto, AC loss measurement of 46 kA-13T Nb/sub 3/Sn conductor for ITER, IEEE Trans. Appiled Supercond. 11 (2001) 1546–1549.
[60] A. Nijhuis, Y. Ilyin, W. Abbas, B. ten Haken, H.H.J. ten Kate, Change of interstrand contact resistance and coupling loss in various prototype ITER NbTi conductors with transverse loading in the twente cryogenic cable press up to 40,000 cycles, Cryogenics (Guildf). 44 (2004) 319–339.